Unimolecular Dissociation Kinetics of Benzene Cluster Ions

Kazuhiko Ohashi, Kei Adachi, and Nobuyuki Nishi*

Department of Chemistry, Faculty of Science, Kyushu University, Hakozaki, Fukuoka 812-81

(Received October 12, 1995)

The "unimolecular" dissociation processes of benzene cluster ions prepared by resonant 2-photon ionization (R2PI) of neutral clusters were investigated by using a time-of-flight mass spectrometer equipped with a reflectron. The dissociation rates were determined for fast-decay processes (k_{fast}) in the acceleration region and slow dissociations (k_{slow}) in the drift region of the spectrometer. The ejection of one neutral molecule was a dominant dissociation channel of small $(C_6H_6)_n^+$ in the drift region; in addition, the ejection of two molecules was observed for $n-2 \geq 14$. These size-specific dissociation channels and the size dependence of the k_{slow} values imply a closing of the first shell of $(C_6H_6)_n^+$ at $n=14$. The magnitude of both k_{fast} and k_{slow} was found to be independent of the excess energy upon R2PI, suggesting rapid cooling of the nascent hot ions by prompt dissociation within the laser focus. For slow dissociation within a well-defined time window, the measured values of k_{slow} were compared with those calculated according to a statistical theory of unimolecular reaction. The comparison deduced the average internal energies of $(C_6H_6)_n^+$ at ca. 1 μs after preparation.

Investigations of the unimolecular dissociation of clusters on a metastable time scale, namely, metastable dissociation, comprise an active area of current research.[1—4] A large number of studies have been conducted concerning the properties of the metastable dissociation of cluster ions produced by either electron-impact ionization or the photoionization of neutral clusters. Such studies have provided information on the energetics, kinetics, and dynamics of dissociation processes of cluster ion species, including rare-gas, molecular, and metal clusters. The metastable dissociation of uniquely selected cluster ions is also an ideal testing ground for statistical theories of unimolecular dissociation.[5]

A related subject in the field of cluster research concerns the origin of magic numbers, a term used to describe the anomalous abundance of certain sizes of clusters in an otherwise smoothly varying cluster distribution. The origin of magic numbers in mass spectra used to be a controversial subject, i.e., some investigators interpreted them as being due to the special structure and stability of neutral clusters, whereas others attributed them to the stability of cluster ions produced during the course of mass analysis.[6,7] However, several studies of Ne,[8] Ar,[9,10] Xe,[11] and H_2O[12] have shown that, at least for van der Waals clusters, the stabilization due to metastable evaporation after the ionization process is the main reason for the occurrence of the anomalous abundance. Well-resolved mass spectra of $(C_6H_6)_n^+$ were reported by several groups, including Whetten and co-workers for sizes up to $n=40$,[13] and Neusser and co-workers up to $n \approx 190$.[14] The magic numbers are seen at $n=14$, 20, 24, and 27 in these mass spectra, although the anomalies are less prominent compared to those of rare-gas clusters. Based on the stability with respect to the evaporative decay, Schriver et al. concluded that these magic numbers result from the high stability of the respective cluster ions.[13] The metastable dissociation of $(C_6H_6)_n^+$ was also studied by Neusser and co-workers,[14—18] Hertel and co-workers,[19] and by our group.[20] Ernstberger et al. found pronounced anomalies in the metastable decay efficiency at $n=14$, 20, 24, and 27.[14] These features were interpreted in terms of shell filling achieved for icosahedral structures about a central dimer ion.[13,14]

Statistical models of the metastable dissociation processes permit a determination of the binding energy of the evaporated species from the dissociation lifetimes and kinetic energy release or from the dissociation rates within a well-defined time window. For example, Conway and Janik determined the binding energies of $(O_2)_n^+$ with $n=2$—5 from the measured rates of dissociation and a semiclassical model for the rate constant.[21] Engelking[22] modified the standard RRK (Rice–Ramsperger–Kassel) theory[5] according to a requirement based on the principle of detailed balance. He applied the modified RRK theory to calculate the binding energies of $(CO_2)_n^+$ and Ar_n^+,[23] using the experimental data of Stace and co-workers.[24,25] However, this method is accompanied by a basic difficulty for cluster ions with a broad distribution of internal energies. Cluster ions produced by the ionization of neutral clusters are usually energy-rich with a broad distribution of internal energies. Bréchignac et al.[26] compared the measured dissociation rates of K_n^+ with those calculated from the modified RRK theory to determine the binding energy. In the course of the calculation, the internal energy distribution for K_n^+ was determined in a recursive way. The distribution was shown to be a function of the time window of the observation.[27] Klots introduced the concept of an "evaporative ensemble" to model ionic clusters.[28—30] He pointed out that the thermodynamic properties of clusters can be extracted by fitting the measured metastable fractions with the estimated heat capacity and Gspann parameter. Since this approach is based on the rate constants from continuum

theory, however, an average evaporation energy common to all cluster sizes studied was applied in fitting the experimental data.[9,30—32] Recently, this method was modified so as to account for individual dissociation energies of different sizes.[33] The modified version was used by Castleman and co-workers to calculate the dissociation energies of xenon,[34] ammonia,[35] and water[36] cluster ions. The approach, according to the evaporative ensemble model, has now become a standard for understanding the evaporative processes occurring in clusters. By using the evaporative ensemble model and an RRKM (Rice–Ramsperger–Kassel–Marcus) theory,[5] Ernstberger et al. determined the dissociation energies of $(C_6H_6)_n^+$ with $4 \leq n \leq 23$.[14,18] In this size range the dissociation energy is smallest for $(C_6H_6)_5^+$, and begins to increase with increasing cluster size, except for step-like drops after $n=14$ and $n=20$.

In our previous studies on the photoinduced fragmentation of $(C_6H_6)_n^+$,[37,38] the parent ions were created through resonant 2-photon ionization (R2PI) of the neutral clusters. No information was available about the internal energy distribution of $(C_6H_6)_n^+$ after R2PI, although such information is necessary to properly interpret the photofragmentation data. In this paper we describe our efforts to estimate the internal-energy distribution of $(C_6H_6)_n^+$, where we monitor the rate of metastable dissociation as a diagnostic of the internal energy. The experiments are performed by subjecting a cluster beam to laser ionization and analyzing the resulting cluster ions in a time-of-flight (TOF) mass spectrometer equipped with an ion reflector. The cluster ions are formed by 1-color R2PI of neutral clusters in the same way as the photofragmentation studies.[37,38] The use of an ion reflector allows us to study the dissociation processes occurring in two different regions of the mass spectrometer: Fast decay processes in the acceleration region of the ion source and slow dissociations in the field-free drift region.[39] The 1-color R2PI method is expected to prepare a set of cluster ions characterized by a broad internal energy distribution. However, rapid relaxation processes in the ion source ensure well-defined internal energies of the ions at the entrance of the drift region. We then measure the rate of the subsequent dissociation in the drift region under carefully controlled conditions. In order to verify the effect of rapid relaxation processes in the ion source, we compare the dissociation rates of the ions formed with different excess energies (through R2PI via different intermediate states). Finally, we apply the modified RRK theory,[22,23] together with the binding energies reported by Ernstberger et al.,[14,18] to estimate the internal energies of $(C_6H_6)_n^+$ with $n=4$—14 at ca. 1 μs after the preparation (0.77 μs for $n=4$ and 1.45 μs for $n=14$).

Experimental

Experimental Setup. Since the details concerning the experimental apparatus have been presented elsewhere,[38,40] only a brief description of the features relevant to the present study is given here. Neutral benzene clusters were formed by expanding a mixture of benzene and argon through a pulsed value (General Valve Series 9) having a 0.80-mm orifice diameter. The total stagnation pressure was ca. 150 kPa (≈1100 Torr). After passing through a skimmer and a collimator, the cluster beam entered a two-stage acceleration region (ion source) of the mass spectrometer (Jordan Co. Angular Reflectron). Figure 1 schematically illustrates the layout of ionization through detection. In the first stage of the ion source, the cluster beam was crossed by an ionization laser beam. A dye laser (Lumonics HyperDYE-300) was pumped with a XeCl excimer laser (Lumonics HyperEX-400) and the output was frequency-doubled in a BBO (β-BaB_2O_4) crystal. The laser system produced light pulses of approximately 6-ns duration at wavelengths necessary for R2PI via either the first single S_1 ($\lambda \approx 260$ nm) state or the second singlet S_2 ($\lambda \approx 210$ nm) state of the neutral clusters (see the next section). The ions formed by R2PI process were accelerated up to ca. 2.2 keV and then introduced into a field-free drift region ($L=1.07$ m). The pressure in the drift region was kept below 10^{-5} Pa to ensure collision-free conditions. In Fig. 1, t_1 stands for the residence time in the first stage of the acceleration region; t_2 and t_3 are the times at the entrance and exit of the drift region, respectively. From the geometrical parameters of the mass spectrometer and the applied voltages to the ion source, the values for t_1, t_2, and t_3 are readily obtained and tabulated in Table 1. The ions were then reflected by a two-stage ion reflector[2,39] situated at the end of the drift region. The first grid of the reflector was held at ground potential. The second and the last grids were biased at U_T and U_K, respectively. The reflector was normally operated in a partial correction mode in order to separate the ions that dissociate during the drift region from the intact ions that remain after entering the drift region.[2,39,41,42] The reflected ions were detected by dual microchannel plates (Galileo 3320). The ion signals received by the detector were amplified through a fast preamplifier (Anritsu MH-648A) and fed into a digital storage oscilloscope (LeCroy 9400). The laser was typically operated at 10 Hz and the TOF spectra were sampled by the accumulation of 2000—5000 laser shots.

Excitation Conditions. One of the purposes of the present work is to compare the metastable dissociations of cluster ions created through R2PI via different intermediate states. Hiraya and Shobatake measured the direct absorption spectra of neutral ben-

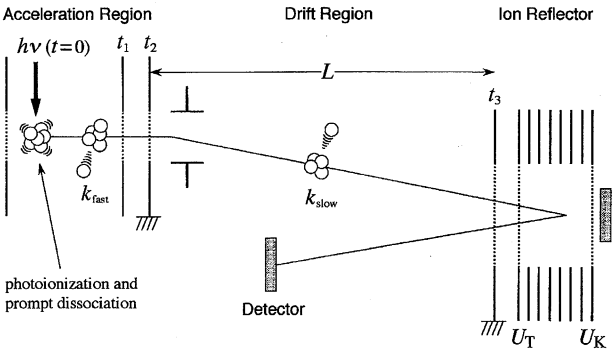

Fig. 1. Schematic illustration of the layout of ionization through detection. Neutral clusters are ionized by a pulsed laser at $t=0$ followed by prompt dissociation of nascent hot ions in the laser focus. The rate coefficient for a fast dissociation process while traveling in the first stage of the acceleration region (until $t=t_1$) is denoted by k_{fast}. Passing through the last grid of the ion source at $t=t_2$, the ions enter the field-free drift region. The rate coefficient for a slow dissociation process in this region (from $t=t_2$ to t_3) is denoted by k_{slow}. The ions are then reflected by the two-stage ion reflector and arrive at the detector.

Table 1. Time Zone for Experimental Observation

n[a]	t_1[b]/μs	t_2[c]/μs	t_3[d]/μs
2	0.45	0.55	21.1
3	0.56	0.67	25.9
4	0.64	0.77	29.9
5	0.72	0.86	33.4
6	0.79	0.95	36.6
7	0.85	1.02	39.5
8	0.91	1.09	42.2
9	0.96	1.16	44.8
10	1.01	1.22	47.2
11	1.06	1.28	49.5
12	1.11	1.34	51.7
13	1.16	1.39	53.8
14	1.20	1.45	55.9
15	1.24	1.50	57.8
16	1.28	1.55	59.7
17	1.32	1.59	61.6
18	1.36	1.64	63.4

a) Cluster size. b) Time after ionization when the ions pass through the middle grid of the ion source. c) Time at the exit of the ion source. d) Time at the entrance of the ion reflector.

zene clusters in a free jet in the 175—225 nm region.[43] Two broad absorption maxima were found at 208 and 185 nm and were assigned to the S_2 and S_3 absorption systems of the clusters, respectively. Resonance enhancement via the S_2 state is considered to be independent of the cluster size, because only broad bands were found in the $S_2 \leftarrow S_0$ excitation spectra.[44] Here, we used 210-nm light to ionize the neutral clusters non-selectively. The S_1 state of the clusters has been extensively studied by several groups. For small clusters with $n=2$—5, discrete sharp features were observed in the $S_1 \leftarrow S_0$ spectra.[16,45,46] Resonance enhancement of particular ion signals is possible when the laser frequency is tuned exactly to the known $S_1 \leftarrow S_0$ transition of the corresponding neutral clusters. For larger clusters, the spectra are broader and less structured. The central positions of the broad 6^1 band near to 260 nm undergo a gradual shift toward longer wavelengths with increasing cluster size.[47] When we operate the laser at wavelengths slightly longer than the sharp $S_1 \leftarrow S_0$ transitions of the small clusters, we can record the mass spectra of all cluster ions simultaneously.

The ionization potential (IP) for the benzene monomer is 9.243 eV.[48] The following IP's for neutral clusters are reported:[49] 8.65±0.01 eV for the dimer, 8.58±0.02 eV for the trimer, 8.55±0.02 eV for the tetramer, and 8.50±0.02 eV for the pentamer. A comparison of these five values shows that a substantial stabilization is achieved for the dimer, whereas further stabilization is small for up to the pentamer. For this reason, the IP's of larger clusters are presumed not to change drastically with increasing cluster size. Thus, 1-color R2PI via the S_1 state at $\lambda = 260$ nm ($2h\nu = 9.54$ eV) produces an excess energy of 0.89—1.04 eV for the dimer through the pentamer and ca. 1.1 eV for larger clusters. The excess energy is partitioned between the kinetic energy of the electrons and the internal energy of the ions. We may assume that the cluster ions are originally produced with an energy content between null and the maximum excess energy, since no information is available about the internal-energy distributions of the ions. This assumption was recently verified for the dimer by a measurement of the photoelectron spectra after R2PI of the neutral dimer.[14] Hot ions with large internal energies may cool via successive evaporation of neutral molecules. For example, the hottest $(C_6H_6)_5^+$ ions, having an initial excess energy of 1.1 eV, can eject up to 3 neutral molecules. Rather cold ions will not have sufficient internal energy to dissociate within the time window of the detection scheme. According to the time evolution described by the evaporative ensemble model,[28—30,33] the cluster set will relax toward an ensemble, the average temperature of which decreases with time. On the other hand, 1-color R2PI via the S_2 state at $\lambda = 210$ nm ($2h\nu = 11.80$ eV) leads to excess energy as large as 3.15 eV, even for the dimer. The nascent cluster ions probably have an internal energy content ranging from 0 to ca. 3.3 eV. We suppose that almost all cluster ions under study are smaller than the originally ionized clusters as a result of the rapid cooling processes.

Results and Discussion

Magic Numbers in Mass Spectra. Figure 2 shows a conventional TOF mass spectrum of benzene cluster ions, which is recorded with a detector behind the ion reflector by setting $U_T = U_K = 0$. In this mode, fragment ions originating from dissociations in the drift region are not distinguished from their precursors because the dissociations do not change the velocity of ions. Consequently, we measure the distribution of the ion population at the entrance of the drift region (at $t = t_2$). Here, the cluster ions are produced by 1-color R2PI via the S_2 state ($\lambda = 210$ nm). The intensity of the ions smoothly decreases along with increasing cluster size, except for magic numbers at $n = 14$ and 20. Schriver et al.[13] observed magic numbers at $n = 14$, 20, 24, and 27 in the mass spectrum of $(C_6H_6)_n^+$ produced by R2PI via the S_3 state ($\lambda = 193$ nm). Recently, Ernstberger et al.[14] compared the mass spectra obtained at high (ca. 10^7 W cm^{-2}) and low ($< 10^5$ W cm^{-2}) laser intensities, following R2PI via the S_1 state ($\lambda = 260$ nm). At high laser intensity, the cluster ions up to $n \approx 120$ were observed and the ion signal decreased monotonically with increasing cluster size. Magic numbers were observed at $n = 14$, 20, 24, and 27. These positions agree with

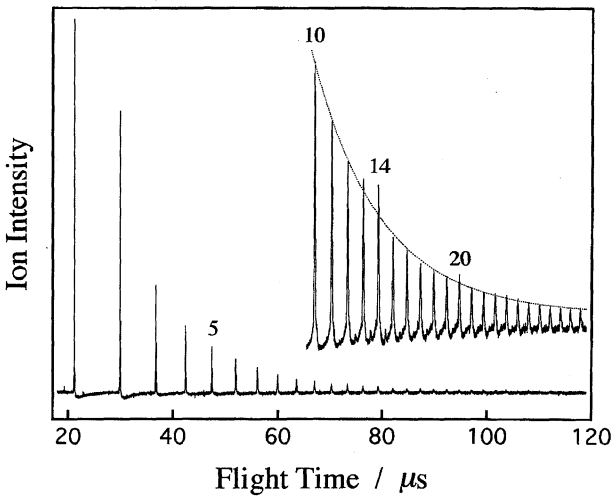

Fig. 2. A conventional time-of-flight mass spectrum of benzene cluster ions after resonant 2-photon ionization at λ = 210 nm. The spectrum of the larger clusters ($n \geq 10$) is recorded with increased sensitivity of the detector. The mass peaks of $(C_6H_6)_n^+$ with $n = 5$, 10, 14, and 20 are labeled.

those found in previous studies. Although the excess energies upon ionization at 2-photon levels differ considerably (4.20, 3.15, and 0.91 eV for R2PI of the dimer via the S_3, S_2, and S_1 state, respectively), the same intensity anomalies were observed independent of the excitation conditions.

Using a reflecting potential screen at the detector end of the mass spectrometer, Schriver et al. found that the benzene cluster ions at the magic numbers are particularly stable with respect to evaporative decay.[13] They concluded that these features result from the high stability of the respective cluster ions, and supposed icosahedral structures about a central dimer ion. Ernstberger et al.[14] pointed out that the small cluster ions with $n < 30$ cannot survive R2PI without fragmentation, even at low laser intensities, and that the fragmentation processes of the ions destroy the initial distribution of neutral clusters. Therefore, evaporative stabilization after ionization is the most likely origin for the occurrence of the intensity anomalies in the mass spectra; also, the magic numbers should reflect the stability of the cluster ions. In the following sections quantitative data are presented for the rates of the evaporative decay processes in two different time windows of the experiment.

Fast Decay in the Ion Source. Hot cluster ions with extremely large internal energies dissociate instantaneously by ejecting neutral molecules. With the present experimental setup, however, we cannot identify the dissociation occurring in the focus of the ionizing laser (we call this process "prompt dissociation" hereafter). A part of the less hot ions dissociate while traveling in the ion source of the mass spectrometer. This delayed dissociation process on the time scale of 10^{-7}—10^{-6} s leads to a flight-time asymmetry in the ion signals on the mass spectrum.[39,41] Figure 3 shows a monomer region of a partially corrected TOF mass spectrum of benzene cluster ions formed via the S_2 state. All of the ions that survived delayed dissociation in the ion source are eliminated from the spectrum by using a suitable set of reflector voltages. The signal consists of a late-arriving tail due to the delayed dissociation of $(C_6H_6)_2^+$ into $C_6H_6^+ + C_6H_6$ in the ion source. We can simulate the profile of the tail by converting the dissociation time into the arrival time.[50] Each of the three theoretical curves in Fig. 3 represents the peak shape calculated for a single exponential decay with a different rate coefficient (k_{fast}). Although the decay process under consideration is not necessarily the single exponential decay, the observed shape can be reasonably reproduced by a theoretical curve with $k_{fast} = 6 \times 10^6$ s^{-1}. The discrepancy at around 31.4—31.6 μs is simply due to the signal of ^{13}C benzene molecules, which interferes with the experimental peak shape. A similar procedure follows for the decay process:

$$(C_6H_6)_n^+ \xrightarrow{k_{fast}} (C_6H_6)_{n-1}^+ + C_6H_6, \quad (1)$$

with n=2—5; the values of k_{fast} are plotted in Fig. 4. The observed values of k_{fast} decrease along with increasing cluster size. At first glance, this tendency concerning the size dependence is in accordance with a prediction by unimolecular rate theories. In this measurement, however, we see the

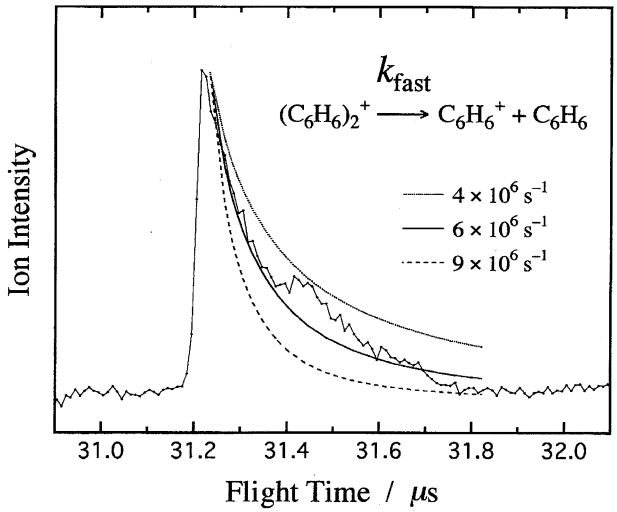

Fig. 3. Monomer region of a partially corrected reflectron mass spectrum of the benzene cluster ions after resonant 2-photon ionization at $\lambda = 210$ nm. The late arriving tail is due to the fast dissociation of $(C_6H_6)_2^+$ into $C_6H_6^+ + C_6H_6$ in the ion source. The experimental profile is compared with three theoretical curves with different values of the rate coefficient k_{fast}. The discrepancy at around 31.4—31.6 μs is due to the signal of ^{13}C benzene molecules, which interfere with the experimental peak shape.

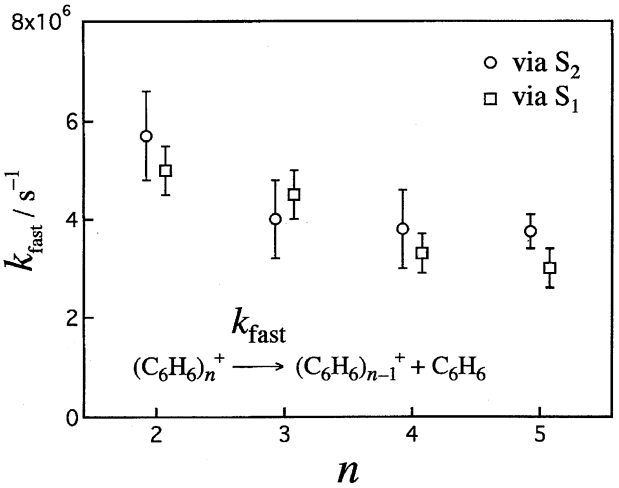

Fig. 4. Rate coefficients for the fast decay processes (k_{fast}) of $(C_6H_6)_n^+$ into $(C_6H_6)_{n-1}^+$ and C_6H_6 for n=2—5. The $(C_6H_6)_n^+$ ions are prepared by resonant 2-photon ionization via the S_1 state at λ =259.4 nm (squares) and via the S_2 state at λ =210 nm (circles). The error bars indicate experimental uncertainties determined from a series of individual measurement.

dissociation of only those ions with lifetimes comparable to the time window of the observation. The magnitude of k_{fast} is governed not only by the microcanonical rate coefficient, but also by the internal-energy distribution of the cluster ions. In order to properly discuss the size dependence of the rate coefficient, we should perform measurements for a series of the clusters with well-defined internal energy.

We restrict ourselves here to a consideration of the excess

energy dependence of the observed values of k_{fast}. The values for ions prepared via the S_2 state agree with those for ions via the S_1 state within the experimental uncertainties, although the excess energies at the 2-photon levels differ considerably from each other (3.15 vs. 0.91 eV for the dimer). Although one may suppose that the difference in the excess energy is simply balanced by the kinetic energy of the photoelectron, we speculate that prompt dissociation processes lead to a similar internal energy distribution regardless of the excess energy. The initial internal energy distribution for an ensemble of ions with a given size is certainly dependent on the excess energy; R2PI via the S_2 state leads to a distribution which is broader than that after R2PI via the S_1 state. However, the ions with large internal energies cannot remain intact without dissociation, and are eventually removed from the ensemble. Thus, the upper limit of the distribution is expected to depend only on the time scale of the observation.[28—30,33] As a result of prompt dissociation, similar distributions of internal energies are achieved independently of the excitation conditions.

In order to examine the effect of prompt dissociation, which we cannot detect directly, on the consecutive fast-decay process under the observation, we compare the decay rate (k_{fast}) of $(C_6H_6)_2^+$ produced by size-selective R2PI at λ =259.0 nm with that by non-selective R2PI at λ =259.4 nm. The wavelength of 259.0 nm exactly coincides with the sharp 6^1 band of the $S_1 \leftarrow S_0$ transition for the neutral dimer; the resulting $(C_6H_6)_2^+$ ions are formed from $(C_6H_6)_2$ without fragmentation. At 259.4 nm, on the other hand, larger clusters are mainly ionized; the $(C_6H_6)_2^+$ ions are formed from larger clusters through the fragmentation. The observed value of k_{fast} for $(C_6H_6)_2^+$ from $(C_6H_6)_2$ is $(8.3\pm1)\times10^6$ s^{-1}, which is larger than that for $(C_6H_6)_2^+$ from the larger clusters (indicated in Fig. 4). For $(C_6H_6)_2^+$ from $(C_6H_6)_2$, a larger fraction of the ensemble remains hot, since cooling by prompt dissociation is not possible.

Metastable Mass Spectra. The prompt dissociation in the laser focus ($k>10^8$ s^{-1}) and the fast decay in the ion source ($k_{fast}\approx10^7$—10^6 s^{-1}) determine the upper limit of the internal energies of cluster ions. As the cluster ions evaporatively cool through these processes, the dissociation extends to longer times. The measurement is then directed to the metastable dissociation processes in the field-free drift region of the mass spectrometer. Figure 5 shows the reflectron TOF mass spectra of benzene cluster ions in a partial correction mode. The lower spectrum is obtained by R2PI at λ =210 nm (via the S_2 state); the upper spectrum is recorded under the same conditions as the lower one, but with λ =259.4 nm (via the S_1 state). The essential features of the two spectra are similar to each other. The spectra comprise a series of two or three slightly shifted peaks, because the ion signals resulting from the metastable dissociation in the drift region,

$$(C_6H_6)_n^+ \xrightarrow{k_{slow}} (C_6H_6)_{n-m}^+ + mC_6H_6, \qquad (2)$$

can be distinguished in partially corrected mass spectra. The abscissa of the figure stands for the size of the product ions

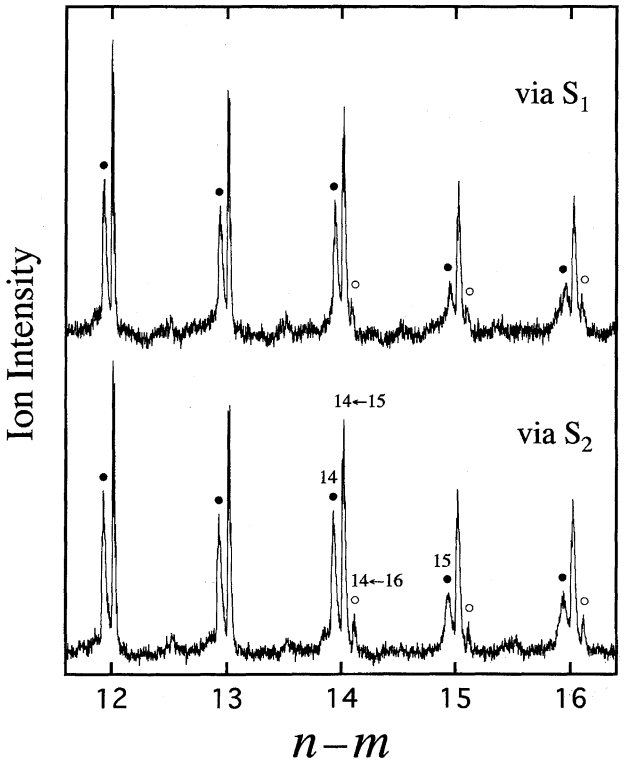

Fig. 5. Partially corrected reflectron mass spectra of benzene cluster ions after resonant 2-photon ionization via the S_2 state (lower) and via the S_1 state (upper). The spectra are composed of a series of two or three slightly shifted peaks resulting from the metastable dissociation in the drift region, $(C_6H_6)_n^+ \rightarrow (C_6H_6)_{n-m}^+ + mC_6H_6$. The abscissa of the figure stands for the size of the product ions. The first peak (marked with ●) is due to the stable ions that remain intact in the drift region. The strong second peak is due to the metastable ions originated from the loss of one neutral benzene molecule (m=1). The third peak (marked with ○) at cluster sizes $n-m\geq14$ is resulting from the loss of two neutral molecules (m=2).

($n-m$). The first peak (marked with ●) is due to "stable ions" that have not undergone any metastable dissociation in the drift region. The strong second peak is due to the metastable ions resulting from the loss of one neutral benzene molecule (m=1) during field-free flight. Metastable decay processes of this type (loss of one neutral molecule) have been found for many cluster ions.[1—4] At cluster sizes $n-m\geq14$, the third peak (marked with ○) can be identified, which originates from the loss of two molecules (m=2). These assignments are made by calculating the flight time of the metastable ions, where the only unknown parameters are the sizes of the precursor and product ions.

A sudden drop is seen in the intensity of stable ions (●) between the cluster sizes n=14 and 15. Being complementary to this drop, there is a growth in the metastable ion signal of 14←15 with respect to the neighboring 13←14 and 15←16 signals. These features point to an anomalously high efficiency for the metastable decay process, $(C_6H_6)_{15}^+ \rightarrow (C_6H_6)_{14}^+ + C_6H_6$. For the precursor $(C_6H_6)_n^+$

ions with $n-2<14$, ion signals corresponding to the loss of two molecules are very weak and just on the order of the noise level. This result suggests a large stability of $(C_6H_6)_{14}^+$ compared to larger cluster ions.

Rate Coefficients of Metastable Dissociations. We calculate the apparent dissociation rates,[8,9,11] assuming an exponential decay behavior within the time window. The rate coefficients can be derived from the integrated intensities of the stable (parent) and metastable (daughter) ions in the mass spectrum. There are several problems which cause an inaccuracy in the measurement of the rate coefficients. First, peaks of the stable and metastable ions overlap with each other (as shown in Fig. 5) when we operate the ion reflector in a mode close to a complete correction.[39,41] In this case, the peak profile is fitted with appropriate functions to decompose the overlapped peaks. Second, we use the ion reflector in the partial correction mode to separate the metastable ions and the stable ions. This operational mode leads to different flight paths and different collection efficiencies of the detector for the metastable and the stable ions.[31] Therefore, a pair of mass spectra is recorded for the metastable and corresponding stable ions, where the voltages on the ion reflector are carefully controlled in order to force the metastable ions to follow the same flight path as the corresponding stable ions.[31]

The effective rate coefficient of the metastable decay processes in the drift region (k_{slow}) is then given by

$$\frac{I_s}{I_s+I_m}=\exp\{-k_{\mathrm{slow}}(t_3-t_2)\} \quad (3)$$

where I_s and I_m stand for the integrated intensities of the stable and metastable ions, respectively. When there exist two dissociation channels, a sequential evaporation mechanism is assumed, i.e., the $n-2\leftarrow n$ ions are assumed to grow up at the expense of the $n-1\leftarrow n$ ions. Then, the metastable intensity (I_m) is calculated from the intensities of both the $n-2\leftarrow n$ and the $n-1\leftarrow n$ ions. Figure 6 displays the rate coefficients (k_{slow}) as functions of the cluster sizes for $(C_6H_6)_n^+$ prepared via the S_2 and the S_1 states. The general tendency is that the rate increases with increasing cluster size. However, the rate stays almost constant in the interval $10\leq n\leq 14$ and suddenly increases from $n=14$ to $n=15$. This anomaly corresponds to an intensity anomaly in the mass spectra (Fig. 5); the intensity drop of the stable ions after $n=14$ is caused by the high dissociation rate of the next cluster ion ($n=15$).

In experimental studies concerning the metastable decay of rare-gas cluster ions, it was found that individual decay rates depends strongly on the cluster size.[8—11] For xenon cluster ions, Xe_n^+ with $n=10$—79, Kreisle et al. measured the dissociation rate on a microsecond time scale.[11] An anomalously high dissociation probability was found for Xe_{14}^+, which is one atom larger than the complete first shell of an icosahedron ($n=13$). One additional atom put on a closed shell is particularly unstable with respect to evaporation. Schriver et al. explained the difference in the magic numbers for benzene and rare gases (14, 20, 24, 27 vs. 13, 19, 23, 26) by considering a tightly bound benzene dimer ion as the core of an icosahedron.[13] The proposed stable structure of $(C_6H_6)_{14}^+$ is then that of a dimer ion with 12 nearly

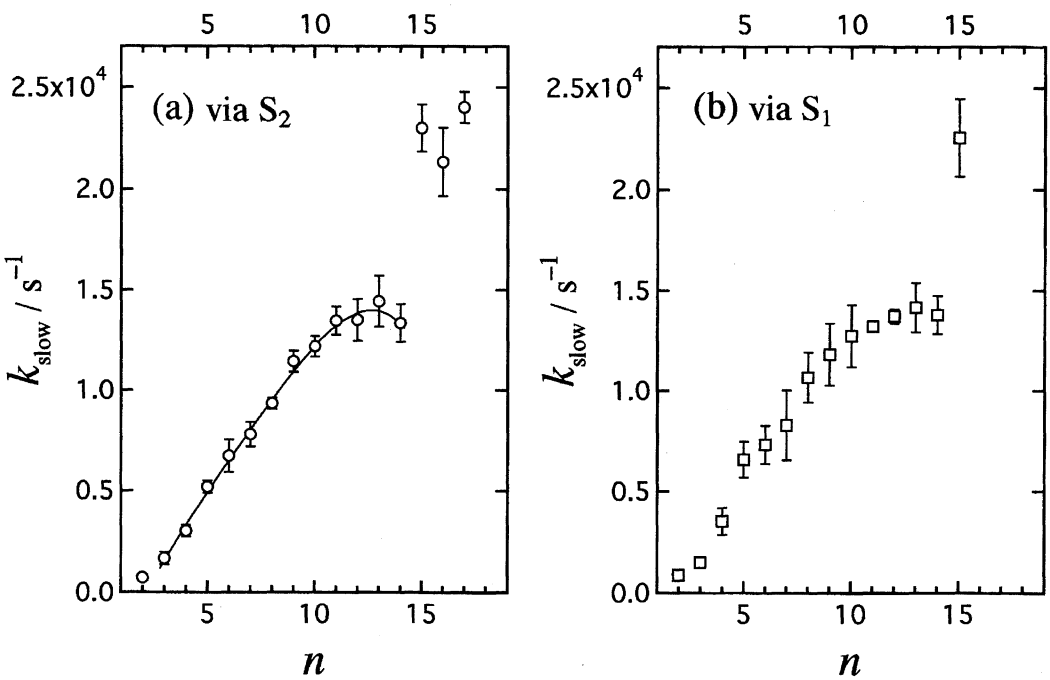

Fig. 6. Rate coefficients for the slow decay processes (k_{slow}) of benzene cluster ions as functions of sizes of the precursors. The ions are prepared by resonant 2-photon ionization via the S_2 state at $\lambda=210$ nm (a) and via the S_1 state at $\lambda=259.4$ nm (b). The error bars indicate experimental uncertainties determined from a series of individual measurement. The solid curve in the left panel is drawn through the theoretical values of k_{slow} calculated with the characteristic temperatures of the precursor ions determined by using Eq. 6.

equivalent surrounding molecules. The size dependence of the dissociation rates shown in Fig. 6 also suggests a closing of the first shell at $n=14$. It should be noted that, in contrast to benzene, no dynamical signature of shell closing has been found for alkylbenzenes (methylbenzene and ethylbenzene)[51] and fluorobenzenes (fluorobenzene, 1,4-difluorobenzene, and hexafluorobenzene).[52]

We now turn to the excess energy dependence of the rate coefficients. It is natural that the values of k_{slow} for the ions prepared via the S_1 state agree with those for the ions via the S_2 state. As noted in the preceding sections, the large excess energy leads to prompt dissociation processes within the laser focus and/or fast decay processes in the ion source; each dissociation step is accompanied by a cooling of the resulting cluster ion. We suppose that almost all cluster ions entering the drift region originate from evaporative cooling processes and that the sizes of the ions are smaller than those of the originally ionized clusters. As a consequence, the internal-energy distribution of these cluster ions is independent of the excitation conditions.

Statistical Theory for Metastable Dissociation. The rate coefficients for the metastable dissociation of cluster ions usually show a monotonic increase with increasing cluster size.[1–4] The behavior is understood within the framework of the evaporative ensemble model developed by Klots.[27–29] In this model, the time evolution of an ensemble of clusters is described by the characteristic temperature of the ensemble and the binding energy and heat capacity of each cluster. In order to estimate unknown parameters in the model, the theoretical prediction is often compared with the experimental observation in terms of the decay fraction, $(I_m/(I_s+I_m))$, rather than the rate coefficient. The decay fraction can be calculated theoretically from the probability distribution ($P(E_{int})$) that the ions have an internal energy of E_{int} and the microcanonical decay rate ($k(E_{int})$) as a function of E_{int}. Ernstberger et al.[14] extracted the dissociation energies of benzene cluster ions from a quantitative analysis of the decay fractions using the evaporative ensemble model. The decay rate ($k(E_{int})$) was calculated using a restricted RRKM model using the reduced phase space of the van der Waals modes. They solved coupled differential rate equations to yield $P(E_{int})$.

We analyze our results in a similar way to estimate the internal energies of the cluster ions. Strictly, an evaporative ensemble cannot be characterized by a single, well-defined temperature, as noted by Klots.[28] For our purpose, however, it is convenient to describe the energy distribution of the ensemble in terms of the temperature. Therefore, the distribution is mimicked by the Boltzmann distribution,

$$P(E_{int}) = (1/N)\rho(E_{int})\exp(-E_{int}/k_B T), \quad (4)$$

where N is the normalization factor, k_B the Boltzmann constant, and T the characteristic temperature of the ensemble. Only the intermolecular modes are taken into account in calculating the density of states $\rho(E_{int})$. The modes include rotations and translations of each monomer unit, providing $6n-6$ ($\equiv s$) degrees of freedom within a $(C_6H_6)_n^+$ cluster. The frequency (ω) of every $6n-6$ mode is set to 20 cm^{-1} for all cluster sizes, since the shape of $P(E_{int})$ is found to be only weakly dependent on the value of ω. The calculated distributions for $(C_6H_6)_n^+$ with n=6, 10, and 14 are displayed in Fig. 7a. The temperature of each cluster is chosen so that the theoretical prediction reproduces the experimental decay fraction. According to the evaporative ensemble model, the width of the energy distribution is approximately equal to the binding energy. The widths of the calculated distributions are 0.09, 0.15, and 0.20 eV for n=6, 10, and 14, respectively, and close to the binding energies of the respective clusters (0.13, 0.18, and 0.21 eV).[14]

The microcanonical rate coefficient ($k(E_{int})$) is calculated using a modified RRK theory of Engelking,[22,23]

$$k_{RRK}(E_{int}) = 8\pi\omega^3(s-1)\mu g\sigma\frac{(E_{int}-E_{bind}-E_{kin})^{s-2}}{(E_{int})^{s-1}}, \quad (5)$$

where μ, g, and σ are the reduced mass, channel degeneracy, and geometrical cross section of the cluster, respectively. E_{bind} is the binding energy of a monomer to the cluster ion

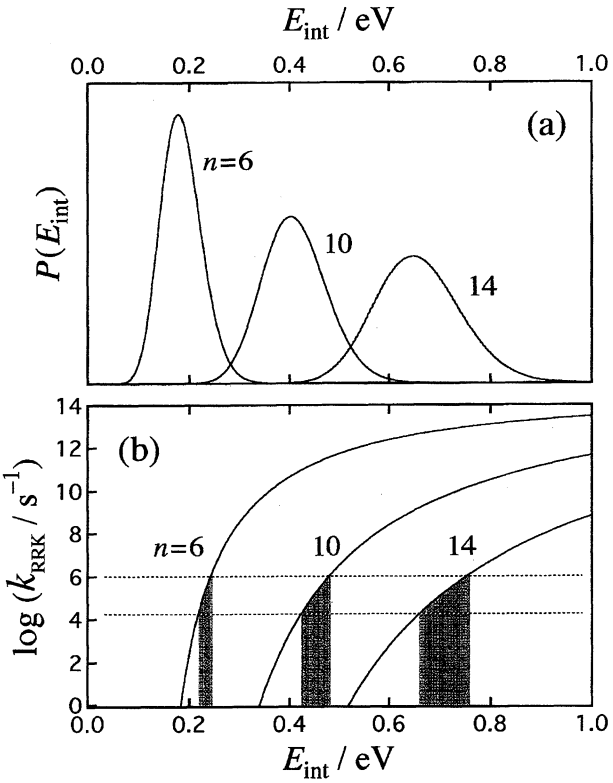

Fig. 7. (a) Internal energy distributions $P(E_{int})$ for $(C_6H_6)_n^+$ with n=6, 10, and 14 calculated by assuming Boltzmann distributions with T=85, 102, and 112 K, respectively. The temperature is chosen so that the theoretical prediction reproduces the experimental decay fraction (see text). (b) Microcanonical rate coefficients k_{RRK} as functions of E_{int} for $(C_6H_6)_n^+$ with n=6, 10, and 14. The rate coefficients are calculated according to a modified RRK theory by using Eq. 5. Two broken lines indicate the range of the rate that leads to the metastable dissociation in the drift region. The shaded areas show the internal energy range leading to the dissociation within the metastable time window.

and E_{kin} is the kinetic energy released during dissociation. The ω and s terms have their previous meanings. We assume that all molecules but two in $(C_6H_6)_n^+$ are available for decay; the remaining two are expected to form a dimeric core that would remain intact. Thus, the channel degeneracy (g) is taken to be $n-2$. The geometrical cross section (σ) is set to $(150\times10^{-16})n^{2/3}$ cm^2. The binding energies are taken from the literature.[14] The average kinetic energy release is reported to be 10—30 meV[19,53] and can be neglected here. Figure 7b demonstrates the calculated rate coefficients for $(C_6H_6)_n^+$ with n=6, 10, and 14. The time zone from t_2 to t_3 determines the range over which the metastable decay will be observed. Because of the relationship between this time zone and the rate coefficient, $1/k$ must lie between t_2 to t_3. For $(C_6H_6)_{10}^+$ as an example, $t_2\approx1\mu$s and $t_3\approx47\mu$s as listed in Table 1. Thus, the range of the rate that leads to the metastable dissociation in the drift region is $6\geq\log(k/s^{-1})\geq4.3$; the two broken lines in Fig. 7b indicate this range of k. Due to the different values of t_2 and t_3 for different sizes, this range shifts slightly to a lower decay rate with increasing size. However, the amount of the shift is very small for the cluster sizes of interest here. What is important in determining the decay fraction is *the internal-energy dependence of the slope of $k(E_{int})$ within the metastable time window and how $k(E_{int})$ overlaps with the internal energy distribution* ($P(E_{int})$). As can be seen in Fig. 7b, the $k(E_{int})$ curve rises steeply for small cluster sizes, whereas the rise of the curve becomes gentler for larger sizes. The shaded areas in Fig. 7b indicate the internal energy range leading to decay within the metastable time window. The range is broader for larger cluster ions. As a consequence, a general increase of the metastable fraction is observed with increasing cluster size.

Quantitatively, we can describe the decay fraction in terms of $P(E_{int})$ and $k(E_{int})$,

$$\frac{I_m}{I_s+I_m}=\int_0^\infty P(E_{int})\left[1-\exp\{-k(E_{int})(t_3-t_2)\}\right]dE_{int}. \quad (6)$$

Equation 6 is the point of contact between experiment and theory. In a calculation of the right-hand side of Eq. 6, we vary the characteristic temperature in order to achieve optimum agreement with the experimental decay fraction on the left-hand side. The solid line in Fig. 6a is drawn through the theoretical values of k_{slow} at the temperatures determined here. Figure 8 shows these temperatures of cluster ions as a function of the cluster size in the range $4\leq n\leq14$. The temperature characterizes the ensemble of the cluster ions at the entrance of the drift region (at $t=t_2$). The $(C_6H_6)_5^+$ ion shows the lowest temperature because it has the smallest binding energy among these sizes. The temperature smoothly rises from 80 K at n=5 to 110 K at n=14. This behavior is probably due to an increase in the binding energy from 0.12 eV for n=5 to 0.21 eV for n=14.[14] Owing to the nature of the evaporative ensemble,[28] the "temperature" is to understood only to signify the energy for these small clusters. Klots also proposed a complementary form of thermometry,[54] which is best applicable to small clusters. The average kinetic energy with which a monomeric unit leaves the surface of a cluster can measure the temperature. Lifshitz and Louage have suggested that the binding energies of the cluster ions can be obtained from accurate measurements of the kinetic energy release.[55] Experiments are now underway on the determination of the kinetic energy released during the metastable dissociation of $(C_6H_6)_n^+$.

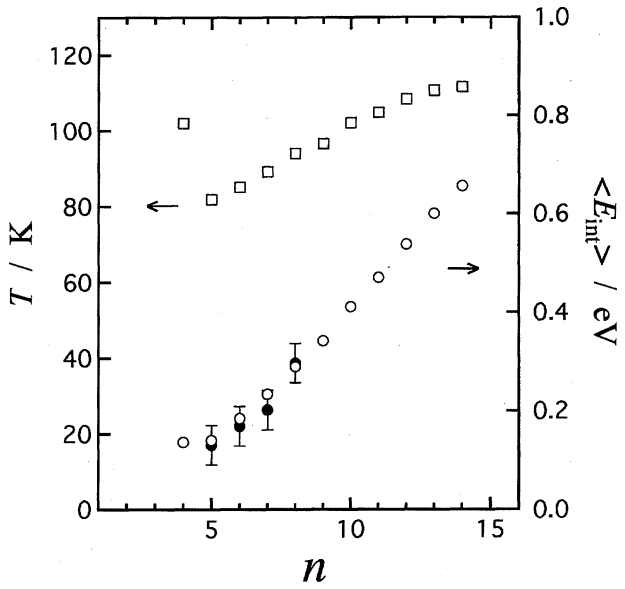

Fig. 8. Characteristic temperatures T (open squares) and average internal energies $\langle E_{int}\rangle$ (open circles) of $(C_6H_6)_n^+$ with n=4—14 at the entrance of the drift region (at $t=t_2$). These values are determined by comparing the calculated decay fractions with the observed ones. The closed circles at n=5—8 stand for the average internal energies derived from photofragmentation data (see text).

Internal Energies of Cluster Ions. The average internal energy ($\langle E_{int}\rangle$) of cluster ions at the entrance of the drift region is also indicated in Fig. 8 (open circles). The average internal energy increases almost linearly from 0.14 eV at n=5 to 0.66 eV at n=14. The internal energy is shared among van der Waals modes of the clusters. The number of these modes increases with increasing cluster size; the larger clusters accommodate a larger energy content, even if the temperatures of the clusters are the same. We should be careful concerning the size-dependence of the internal energy content when we discuss any property of cluster ions as a function of size.

Finally, let us use a different approach to estimate the average internal energy of the cluster ions. In recent publications,[37,38] we reported on photofragmentation studies concerning cluster ions from $(C_6H_6)_3^+$ to $(C_6H_6)_8^+$ at photon energies of between 0.5 and 3.0 eV. The size distributions of the fragment ions were determined and characterized by the parameter $\langle N\rangle$, the average number of neutral molecules ejected following photoexcitation. For $(C_6H_6)_n^+$ with n=5—8, the $\langle N\rangle$ values increase linearly with increasing photon energy ($h\nu$). Extrapolation of the lines for n=5—8 to $h\nu$=0 eV gives an idea about the internal energies of the parent ions. If we regard the value of $\langle N\rangle$ at $h\nu$=0 eV as the probability that the parent ions have internal energies

larger than the binding energy, we can then estimate the internal energies of the ions. The average internal energies obtained in this way are also plotted in Fig. 8 (closed circles). These values are in agreement with those determined from the metastable decay fractions using Eq. 6. We will use the information obtained here to analyze the previous photofragmentation data in further detail.

Conclusions

A major problem inherent in studies using cluster ions is the difficulty to measure the internal energy of size-selected ensembles. Cluster ions are often generated with a large amount of excess energy upon ionization, and cool by subsequent evaporation. We have encountered this situation as usual in our photofragmentation studies of size-selected benzene cluster ions. In this paper, we have shown that the characteristic temperature of the cluster ions can be extracted from a measurement of the rate of metastable dissociations. The average internal energy is shown to increase almost linearly with increasing cluster size from n=5 to 14. The density of states at a given energy increases with the number of modes and, thus, the cluster size. Consequently, the internal energy content greatly changes with the cluster size, even if the clusters have a common temperature. We should be careful concerning the size-dependence of the internal energy content when we discuss any property of cluster ions as a function of size.

Studies on the metastable dissociation of benzene cluster ions were started in collaboration with Professor H. Shinohara (Nagoya University). We thank Professor H. Shinohara for his helpful suggestions.

References

1) T. D. Märk and O. Echt, in "Clusters of Atoms and Molecules II," ed by H. Harberland, Springer-Verlag, Berlin (1994), p. 154.
2) S. Wei and A. W. Castleman, Jr., *Int. J. Mass Spectrom. Ion Proc.*, **131**, 233 (1994).
3) C. Lifshitz, in "Cluster Ions," ed by C. Y. Ng, T. Bear, and I. Powis, John Wiley & Sons, Chichester (1993), p. 121.
4) A. J. Stace, *Org. Mass Spectrom.*, **28**, 3 (1993).
5) M. F. Jarrold, in "Clusters of Atoms and Molecules," ed by H. Harberland, Springer-Verlag, Berlin (1994), p. 163.
6) T. D. Märk and A. W. Castleman, Jr., *Adv. Atom. Mol. Phys.*, **20**, 65 (1985).
7) T. D. Märk, *Int. J. Mass Spectrom. Ion Proc.*, **79**, 1 (1987).
8) T. D. Märk and P. Scheier, *Chem. Phys. Lett.*, **137**, 245 (1987).
9) P. Scheier and T. D. Märk, *Int. J. Mass Spectrom. Ion Proc.*, **102**, 19 (1990).
10) P. G. Lethbridge and A. J. Stace, *J. Chem. Phys.*, **89**, 4062 (1988).
11) D. Kreisle, O. Echt, M. Knapp, and E. Recknagel, *Rhys. Rev. A*, **33**, 768 (1986).
12) O. Echt, D. Kreisle, M. Knapp, and E. Recknagel, *Chem. Phys. Lett.*, **108**, 401 (1984).
13) K. E. Schriver, A. J. Paguia, M. Y. Hahn, E. C. Honea, A. M. Camarena, and R. L. Whetten, *J. Phys. Chem.*, **91**, 3131 (1987).
14) B. Ernstberger, H. Krause, and H. J. Neusser, *Ber. Bunsenges. Phys. Chem.*, **97**, 884 (1993).
15) A. Kiermeier, B. Ernstberger, H. J. Neusser, and E. W. Schlag, *Ber. Bunsenges. Phys. Chem.*, **92**, 437 (1988).
16) A. Kiermeier, B. Ernstberger, H. J. Neusser, and E. W. Schlag, *Z. Phys. D*, **10**, 311 (1988).
17) A. Kiermeier, B. Ernstberger, H. J. Neusser, and E. W. Schlag, *J. Phys. Chem.*, **92**, 3785 (1988).
18) H. Krause, B. Ernstberger, and H. J. Neusser, *Ber. Bunsenges. Phys. Chem.*, **96**, 1183 (1992).
19) J. D. Coffman, M. Gallmann, and I. V. Hertel, *Z. Phys. D*, **12**, 297 (1989).
20) H. Shinohara, H. Sato, F. Misaizu, K. Ohashi, and N. Nishi, *Z. Phys. D*, **20**, 197 (1991).
21) D. C. Conway and G. S. Janik, *J. Chem. Phys.*, **53**, 1859 (1970).
22) P. C. Engelking, *J. Chem. Phys.*, **85**, 3103 (1986).
23) P. C. Engelking, *J. Chem. Phys.*, **87**, 936 (1987).
24) A. J. Stace and A. K. Shukla, *Chem. Phys. Lett.*, **85**, 157 (1982).
25) A. J. Stace, *J. Chem. Phys.*, **85**, 5774 (1986).
26) C. Bréchignac, Ph. Cahuzac, J. Leygnier, and J. Weiner, *J. Chem. Phys.*, **90**, 1492 (1989).
27) C. Bréchignac, Ph. Cahuzac, F. Carlier, M. de Frutos, and J. Leygnier, *J. Chem. Soc., Faraday Trans.*, **86**, 2525 (1990).
28) C. E. Klots, *Nature*, **327**, 222 (1987).
29) C. E. Klots, *Z. Phys. D*, **5**, 83 (1987).
30) C. E. Klots, *J. Phys. Chem.*, **92**, 5864 (1988).
31) S. Wei, W. B. Tzeng, and A. W. Castleman, Jr., *J. Chem. Phys.*, **93**, 2506 (1990).
32) Y. Ji, M. Foltin, C. H. Liao, and T. D. Märk, *J. Chem. Phys.*, **96**, 3624 (1992).
33) C. E. Klots, *Z. Phys. D*, **21**, 335 (1991).
34) S. Wei, Z. Shi, and A. W. Castleman, Jr., *J. Chem. Phys.*, **94**, 8604 (1991).
35) S. Wei, K. Kilgore, W. B. Tzeng, and A. W. Castleman, Jr., *J. Phys. Chem.*, **95**, 8306 (1991).
36) Z. Shi, J. V. Ford, S. Wei, and A. W. Castleman, Jr., *J. Chem. Phys.*, **99**, 8009 (1993).
37) Y. Nakai, K. Ohashi, and N. Nishi, *Chem. Phys. Lett.*, **233**, 36 (1995).
38) K. Ohashi, Y. Nakai, and N. Nishi, *Laser Chem.*, **15**, 93 (1995).
39) U. Boesl, R. Weinkauf, and E. W. Schlag, *Int. J. Mass Spectrom. Ion Proc.*, **112**, 121 (1992).
40) K. Ohashi and N. Nishi, *J. Chem. Phys.*, **95**, 4002 (1991).
41) H. Kühlewind, H. J. Neusser, and E. W. Schlag, *Int. J. Mass Spectrom. Ion Proc.*, **51**, 255 (1983).
42) O. Echt, P. D. Dao, S. Morgan, and A. W. Castleman, Jr., *J. Chem. Phys.*, **82**, 4076 (1985).
43) A. Hiraya and K. Shobatake, *Chem. Phys. Lett.*, **178**, 543 (1991).
44) H. Shinohara and N. Nishi, *Chem. Phys.*, **129**, 149 (1989).
45) J. B. Hopkins, D. E. Powers, and R. E. Smalley, *J. Phys. Chem.*, **85**, 3739 (1981).
46) K. S. Law, M. Schauer, and E. R. Bernstein, *J. Chem. Phys.*, **81**, 4871 (1984).
47) M. Y. Hahn, A. J. Paguia, and R. L. Whetten, *J. Chem. Phys.*, **87**, 6764 (1987).
48) L. A. Chewter, M. Sander, K. Müller-Dethlefs, and E. W. Schlag, *J. Chem. Phys.*, **86**, 4737 (1987).
49) H. Krause, B. Ernstberger, and H. J. Neusser, *Chem. Phys.*

Lett., **184**, 411 (1991).
50) H. Kühlewind, A. Kiermeier, and H. J. Neusser, *J. Chem. Phys.*, **85**, 4427 (1986).
51) K. Adachi, K. Ohashi, and N. Nishi, unpublished results.
52) M. Miwa, H. Shinohara, and H. Sato, unpublished results; M. Miwa, Thesis for M. Eng., Mi'e Univ., 1991.
53) K. Ohashi and N. Nishi, unpublished results.
54) C. E. Klots, *Acc. Chem. Res.*, **21**, 16 (1988).
55) C. Lifshitz and F. Louage, *Int. J. Mass Spectrom. Ion Proc.*, **101**, 101 (1990).